Energy Reports 6 (2020) 3051–3066

Contents lists available at ScienceDirect

Energy Reports

journal homepage: www.elsevier.com/locate/egyr

Performance improvement of a new proposed Savonius hydrokinetic turbine: a numerical investigation

Ramin Alipour [a], Roozbeh Alipour [a,*], Farhad Fardian [a], Seyed Saeid Rahimian Koloor [b,c], Michal Petrů [b]

[a] Department of Mechanical Engineering, Mahshahr Branch, Islamic Azad University, Mahshahr, Iran
[b] Institute for Nanomaterials, Advanced Technologies and Innovation (CXI), Technical University of Liberec (TUL), Studentska 2, Liberec, 461 17, Czech Republic
[c] School of Mechanical Engineering, Universiti Teknologi Malaysia, 81310, Johor Bahru, Johor, Malaysia

ARTICLE INFO

Article history:
Received 29 May 2020
Received in revised form 25 September 2020
Accepted 31 October 2020
Available online 9 November 2020

Keywords:
Savonius turbine
Tidal energy
Blade geometry
Torque coefficient
Power efficient
Thrust coefficient

ABSTRACT

Computational fluid dynamic analysis was conducted with a new proposed Savonius hydrokinetic turbine with a parabolic blade shape specifically geared toward a small-scale power extraction. This parabolic blade geometry was developed by manipulating a couple of disparate kinds of blades in the recent past i.e. semicircular and arc shaped followed by a straight arc. The developed hydrokinetic turbine was tested numerically in a symmetric channel and its performance was evaluated concerning the power, thrust and torque coefficients. Simulations were also implemented with two other mentioned blades. The effects of Reynolds number at different tip speed ratios on the dynamic and static performance of all three models were discussed as well. The present investigation demonstrated a gain of 7.7% and 12% in maximum power coefficient with the new proposed Savonius hydrokinetic turbine by parabolic blade shape than that of the arc shaped followed by a straight arc and semicircular, respectively. Likewise, for this new proposed turbine, the maximum value of static torque coefficient improved by 4% and 25.8% than that of the arc shaped followed by a straight arc and semicircular, severally. For all three simulated blade profiles, the best performance was experienced at an optimum value of tip speed ratio 0.98 and Reynolds number 2×10^5. However, the new proposed turbine at all Reynolds numbers and tip speed ratios in the scope of this research showed a better performance than the other simulated models.

1. Introduction

The increase in the use of fossil fuels results in extreme CO_2 emission (Han et al., 2018) with the consequences such as climate changes (Alipour et al., 2020), instabilities in the world energy price (Roy and Saha, 2013b) and also pollution (Ramar et al., 2018). In this context, renewable energy systems are becoming remarkable important due to reliability (Mercier et al., 2020), efficiency (Mohamed et al., 2010), sustainability (Owusu and Asumadu-Sarkodie, 2016), application in hybrid and electric vehicles to have means of storing energy and their potential to decrease environmental problems (Chatzirodou et al., 2019). Nowadays, several countries are investing in the potential of renewable energy and related infrastructures all over the globe either as a pilot or industrial scales (Sawin et al., 2018). Since the early 1970s, a broad range of advancements has been reported in the case of diverse renewable energy resources such as solar, wave, wind, hydrokinetics (river streams, tidal currents), etc. (Roy and Saha, 2013a). Among these methods and based on turbine usage, wind and water are both abundant, clean, efficient and promising energy resources for off-grid power generation at zero fuel cost (Talukdar et al., 2018). Considering the performance principles, hydrokinetic and wind turbines are generally in common and can be categorized into two well-known classes, i.e. horizontal and vertical axis turbines (Liu et al., 2017). The horizontal axis turbine type rotates around a horizontal axis and the rotor is placed parallel to the flow while the vertical axis turbines generate power by rotating around the vertical axis with an orthogonal shaft across the flow (Michelet et al., 2020). Although horizontal turbines have more capability to extract energy, however based on the material (Alipour and Nejad, 2016) and their manufacturing method (Najarian et al., 2019) it is very cost-effective to use the vertical axis turbine for small-scale and shallow water sites (Khan et al., 2009a).

There are several fabricated vertical axis turbines (Khan et al., 2009a) e.g. Darrius (Antheaume et al., 2008; Rossetti and Pavesi, 2013), Gorlov (Gorlov, 1998) and Savonius, etc. (Al-Dabbagh and

* Corresponding author.
E-mail address: r.alipour@mhriau.ac.ir (R. Alipour).

https://doi.org/10.1016/j.egyr.2020.10.072

Nomenclature

μ	Dynamic viscosity of fluid
ρ	Fluid density
ω	Angular velocity
A	Swept area of turbine
A_d	Axial distance of the blades
CFD	Computational fluid dynamic
Cp	Power coefficient
C_{Pmax}	Maximum Power coefficient
C_T	Torque coefficient
C_{TH}	Thrust coefficient
C_{TS}	Static Torque coefficient
D	Turbine diameter
e	Overlap distance of the blades
H	Height of turbine
NCSHT	New conventional Savonius hydrokinetic Turbine
NPSHT	New proposed Savonius hydrokinetic turbine
P_G	Generative power of turbine
P_H	Hydraulic energy from water
R	Radius of turbine
Re number	Reynolds number
SHT	Savonius hydrokinetic turbine
SSHT	Savonius style hydrokinetic Turbine
SWT	Savonius wind turbines
TSR	Tip speed ratio
URANS	Unsteady Reynolds Averaged Navier Stokes
V_{in}	Inlet velocity

Yuce, 2018). Savonius turbine is one of the most popular turbines in both cases of hydrokinetic and wind applications due to the cost-effectiveness, low noise (Afungchui et al., 2010) and environmental side-effects, and ease of fabrication and installation in comparison with the horizontal axis turbines (Kumar and Saini, 2016). Besides, they are simple to design so that their conventional model is composed of a couple of semicircular blades (Ferrari et al., 2017). This type of turbine works based on the drag force and its performance is independent of flow direction (Akwa et al., 2012b). Nevertheless, Savonius turbines are somehow suffering a lack of power generation (Menet, 2013) which makes them needful to improve their performance through manipulating in geometrical design (Sivasegaram, 1978).

Early researches on Savonius wind turbines (SWTs) were focused on obtaining the real value of maximum power coefficient (C_{Pmax}) that can be observed for instance in Fujisawa and Gotoh (1994). Also, investigation of the performance of SWT in different blade numbers and configurations has been the area of interest for several researchers such as Mahmoud et al. (2012) and Wenehenubun et al. (2015). However, in recent years, many researchers have tried to enhance the efficiency of Savonius wind and hydrokinetic turbines, by modifying the geometry of the blades (Emmanuel and Jun, 2011), using deflector plates and ducts (Benesh, 1996). For example, Kamoji et al. (2009), conducted experimental research on a single stage SWT by modifying the baled geometry at different Reynolds numbers (Re) and showed the modified SWT has the best performance at Re 150,000. In similar researches, Alom et al. (2016) and Banerjee et al. (2014) implemented a computational investigation on the operation of SWTs with different blade geometries and proved that the performance of elliptical blade geometry is better than the semicircular blades. Recently, it has been reported that using the spline blade geometry increases the obtained power coefficient in compression with the conventional semicircular blades (Mari et al., 2017).

Since the past decade, research on the Savonius hydrokinetic turbine (SHT) has taken a notable leap. Some creative ideas such as presented by Faizal et al. (2010) on the use of orbital motion existed in hydro waves showed that the enhancement in height and frequency of the waves can boost the angular velocity of the SHT. Yaakob et al. (2012) and Sarma et al. (2014) studied the performance of a 2-bladed and 3-bladed semicircular SHTs, respectively and tried to find an optimal value for tip speed ratio (TSR) in which the C_{Pmax} can be achieved. Besides, a part of the researchers investigated distinctive performance improvement methods e.g. employing multiple stages deflectors or blade geometries. Golecha et al. (2011) and Kailash et al. (2012) carried out a series of tests to enhance the performance of a modified 2-bladed SHT using a deflector plate located at an optimum place. Results showed using the deflector plate, not only a 50% increase in C_{Pmax} can be achieved, but also this C_{Pmax} is obtained at a higher value of TSR. In a different study, Nakajima et al. (2008) experimentally demonstrated that the power coefficient (C_P) for a SHT is able to be improved using double stage configuration of the blades. The conclusion of the recent paper was in good agreement with Khan et al. (2009b) results. Another experimental investigation was reported by Patel et al. (2017) in which, the overlap ratio and aspect ratio effects on the performance of a SHT was evaluated.

Although the above-mentioned researches on SHT are mostly experimental based and valuable, however, the test plans with a lot of designs and rectifications are costly and dangerous to some extent. Thus, numerical approaches (Alipour, 2011; Alipour and Najarian, 2011; Alipour et al., 2018, 2009) such as computational fluid dynamic (CFD) has been taken for the analysis by several researchers. Elbatran et al. (2017), numerically investigated using a duct to modify the performance of a single stage SHT. To enhance the performance, Kumar and Saini (2017) indicated that by twisting the blades around 12.5°, the C_{Pmax} of a SHT increases considerably. Ferrari et al. (2017) showed that in a similar condition, the C_{Pmax} obtained from a three-dimensional (3-D) CFD analysis is lower than that of a two-dimensional (2-D) simulation. In the case of 2-D simulations, Nasef et al. (2013) revealed that among the different present turbulence models, the results of CFD analysis employing the SST k-ω is more compatible with the experimental outputs.

Although the Savonius turbine has been basically designed for harnessing energy from wind, however as literature showed, there is a big motivation for the researchers to employ it as a hydrokinetic energy extractor device. The flow regimes around the SHTs and SWTs quite dissimilar due to the distinctive nature of the wind flow and the water flowed in an open channel. While the wind flow is predominantly generated due to the pressure difference, water flow is commonly governed due to gravity (Patel et al., 2017). Likewise, the greater power density of water makes the SHT as a spotlight for the researchers. The subtle point is that, though there seems the performance of SHT may be enhanced with the use of axillary equipment e.g. deflector (Golecha et al., 2011), ducts (Elbatran et al., 2017) etc., nonetheless, such additional devices lead to more complexity of the turbine system especially in the phases of fabrication and installation. Hence, the current study attempts to introduce a new proposed conventional SHT with respect to change in the blade design factors so that it has far more acceptable performance than that of reported in the literature. In order to meet the

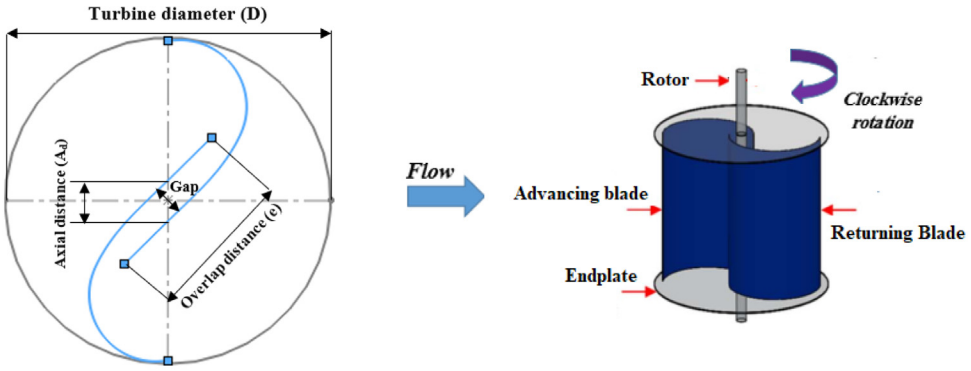

(a) Terminology from Top view (b) 3-D view, adopted from [11]

Fig. 1. Schematic of a SHT.

Table 1
Design specifications of SHTs.

Turbine parameters	Type of SHT		
	NCSHT (Talukdar et al., 2018)	SSHT (Roy and Ducoin, 2016; Roy and Saha, 2015)	NPSHT
D (mm)	250.0	250.0	250.0
e (mm)	37.5	112.5	82.5
A_d (mm)	37.5	30.0	35.0
Height to diameter (AR)	1.0	1.0	1.0

mentioned objective, initially, the performance of a semicircular 2-bladed SHT proposed by Talukdar et al. (2018) is simulated and the torque, thrust coefficient (C_{TH}) and C_P as the performance indicators at different Re are numerically computed. Secondly, a similar scenario is conducted for a recently developed 2-bladed SWT reported as high wind energy capturing capacity (Roy and Ducoin, 2016; Roy and Saha, 2015), but immersed in the water to explore its hydrodynamic performance. Finally, a new 2-bladed SHT is proposed and its performance is investigated in terms of the mentioned indicators with comparison to the initial and second steps. The hydrodynamic performance of models is evaluated via CFD simulations using ANSYS-FLUENT commercial software. Results of simulations for all models are validated against the experimental data presented in Talukdar et al. (2018).

2. Terminology of a 2-bladed Savonius turbine

A SHT consists of rotating parts e.g. blades and endplates, which are assembled around a rotor in the center of the turbine. If a 2-bladed SHT as shown in Fig. 1 is considered, the blades are named as advancing and returning blades. In this type of SHT, rotation mainly comes to pass by the drag force generated between the concave and convex sides of the blades. Further, the lift force as well plays a role to provide the net torque at different rotational positions. It can be expressed that; the advancing blade is subjected to greater drag force than that of the returning blade and thus a positive torque can be obtained. However, it is important to set the negative torque caused by the drag force on the returning blade so that it always stays minimum.

3. Scope of the present research

As per mentioned in the literature, SHTs have several positive points e.g. better self-starting capability and flexible design promises (Roy and Saha, 2014). However, the conventional type of them is reported to have less efficiency than that of its counterpart (Roy and Saha, 2013c). That is the motivation for the present authors toward more improvements in the earlier designs. Among several modified SHT models proposed in the literature, Talukdar et al. (2018) introduced a new conventional Savonius hydrokinetic turbine (NCSHT) with a semicircular blade profile that had higher C_P as compared to the semi-elliptical model offered in Alom et al. (2016). Moreover, digging the literature unveils a new Savonius style wind turbine (Roy and Saha, 2015; Roy, 2014) which has been reported to have more performance as compared to the Benesh type (Benesh, 1996), and modified Batch type (Roy and Saha, 2013a; Roy and Ducoin, 2016; Roy and Saha, 2013c). The recent model with Arc shaped followed by a straight arc blade profile was initially designed for operating in the wind; however, its performance has not ever been checked as a hydrokinetic turbine. Since the scope of this study is covered the hydro performance of turbines, the authors are going to check the performance of this wind turbine in the water area and thus it is named the Savonius style hydrokinetic turbine (SSHT). Considering the mentioned reasons, these two models i.e. NCSHT and SSHT were selected and the performance of a new proposed model which is supposed to be presented in this research is compared to them. Dimensions and schematics of these selected turbines are shown in Fig. 2.

According to the literature, it sounds that manipulating the overlap distance (e) and axial distance (A_d) may serve as a useful parameter to enhance the performance of a SHT (Roy and Saha, 2013b,a; Benesh, 1996; Kamoji et al., 2009; Roy and Saha, 2013c). In addition, several researches (Benesh, 1996; Kamoji et al., 2009; Alom et al., 2016; Banerjee et al., 2014; Roy and Saha, 2015) can be found in which, a part of the blade trailing edge has been designed straight. Though it has not been expressed explicitly in the reports, it seems to be an effective tool for increasing performance and torque extracted from a SHT. So, a new proposed Savonius hydrokinetic turbine (NPSHT) with a parabolic blade profile is presented in this study in which, all mentioned issues i.e. partial straightness of blade profile, e and A_d are considered. Thus, an attempt is conducted to improve the performance of the SHTs. Dimensions and schematics of NPSHT are displayed in Fig. 3. The design parameters for all three models are tabulated in Table 1. In this study, the selection of turbine rotor dimension and aspect ratio (AR) has been adopted from Talukdar et al. (2018). The aspect ratio (AR) mentioned in Table 1 was not used in any

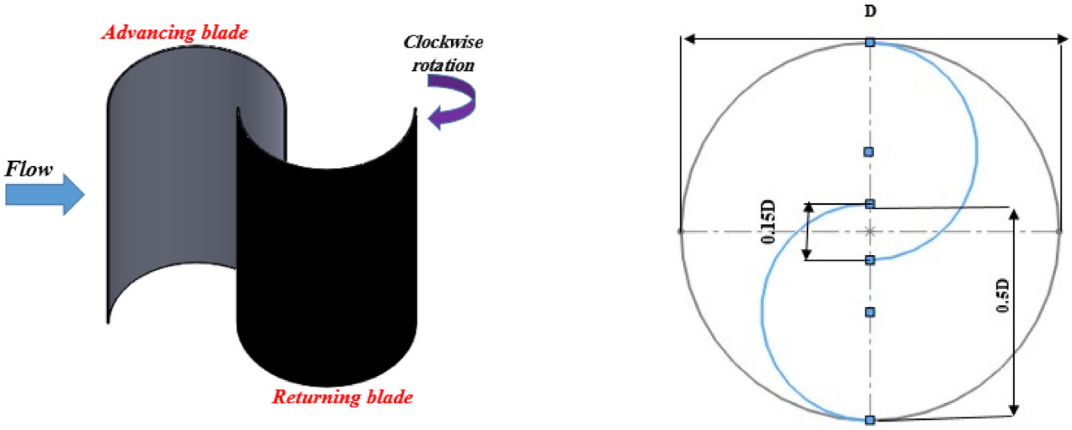

(a) Profile and dimensions of NCSHT [11]: semicircular

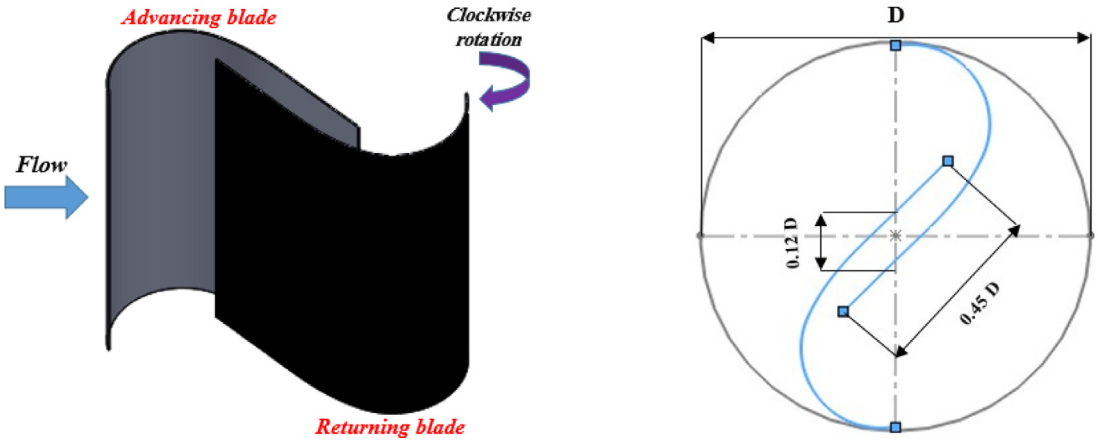

(b) Profile and dimensions of SSHT [51, 52]: arc shaped followed by a straight arc

Fig. 2. Profile and dimensions of SHTs taken from the ligature.

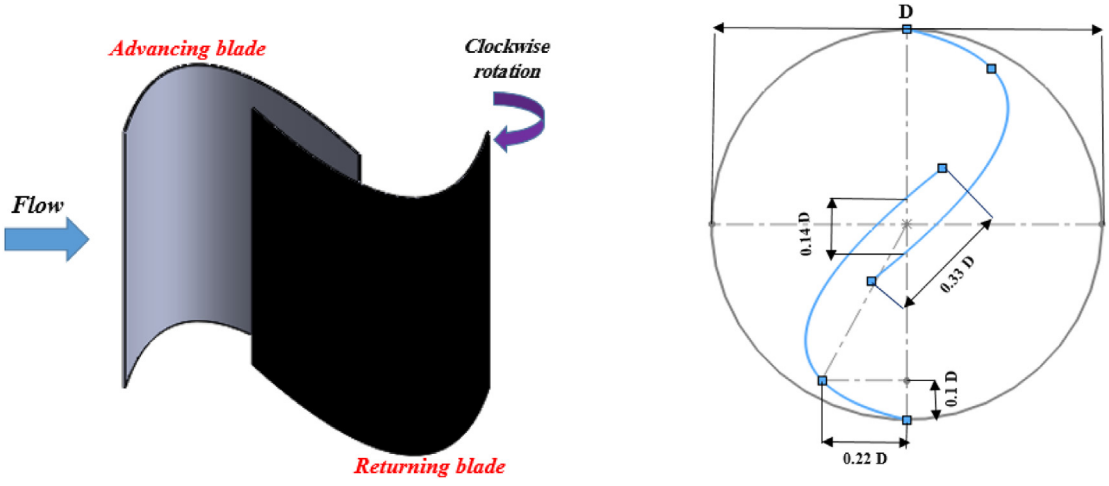

Fig. 3. Profile and dimensions of NPSHT: parabolic shaped.

part of this 2D simulation. However, for those researchers who are interested in fabrication NPSHT, it is useful to know that, an AR < 1.5 is often suitable for Savonius turbines for achieving structural stability (Roy and Saha, 2013a; Talukdar et al., 2018; Abraham et al., 2011). A numerical investigation based on the CFD then is carried out for all three models in which the values of C_P and torque coefficients are extracted at different Re numbers and TSRs.

4. Computational procedure

Based on the proven capability of CFD method to analyze the wide range of fluid flow problems, this method was used in the

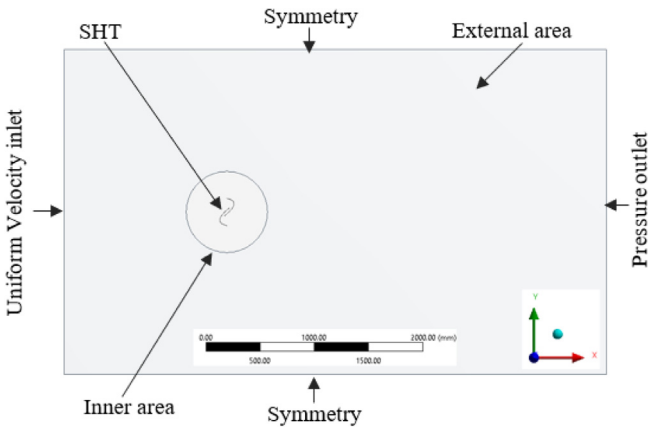

Fig. 4. Boundary condition on the computational domain.

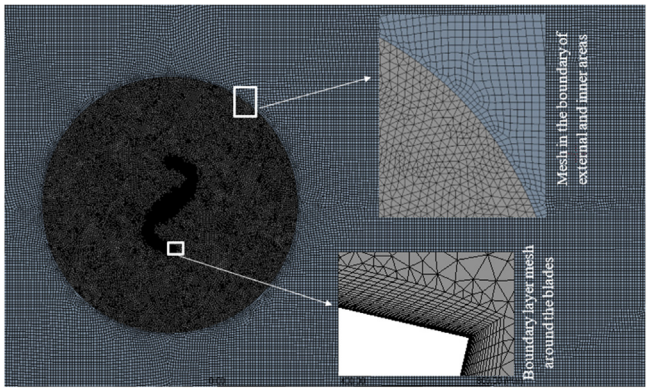

Fig. 5. Close up view of mesh in different regions of the computational domain.

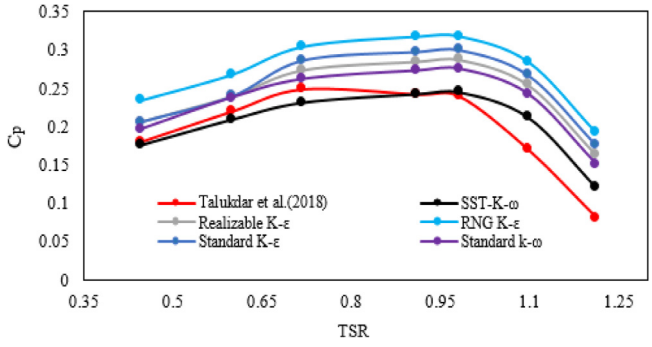

Fig. 6. Experimental measured C_P from Talukdar et al. (2018) versus calculated C_P from the present CFD model based on different turbulence models for NCSHT.

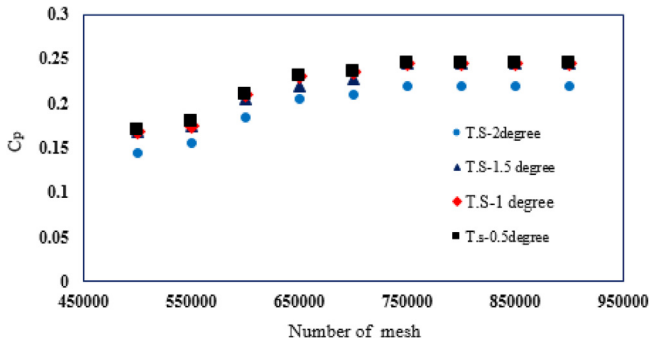

Fig. 7. C_P vs. the number of mesh for different time steps based on the degree of turbine rotation.

present study. Since, in this research, all SHT models are symmetrical along their vertical axis, the 2-D simulations have been conducted to determine the performance of turbines. This strategy has been reported to consume lower computational time with acceptable accuracy (Tian et al., 2015; Rogowski and Maroński, 2015; Altan and Atılgan, 2008). The finite volume method with sliding mesh technique in the bed of ANSYS-FLUENT software was used for the simulations. Among the large number of turbulence models applied for simulating this type of problem (Zhou and Rempfer, 2013), the SST k-ω turbulence model was employed since it is appropriated to model the flow where a precise boundary layer is needed. This turbulence model has been frequently reported to capture a broad range of flows such as adverse pressure gradients, flow around airfoils, rotating flows (Talukdar et al., 2018; Roy and Ducoin, 2016; Menter, 1994). Unsteady Reynolds Averaged Navier Stokes (URANS) equation using the Coupled algorithm (Saeed et al., 2019; Lanzafame et al., 2014) (pressure–velocity) (Saeed et al., 2019; Lanzafame et al., 2014) was utilized for computations. Second order upwind method (Mohamed et al., 2010; Elbatran et al., 2017; Saeed et al., 2019) was applied for the discretization of convective equations. For the simulation of a SHT under unsteady flows, time step (Δt) is very important so that using the large time step causes unrealistic results (Kumar and Saini, 2017). It is suitable to set Δt according to TSR values (Ferrari et al., 2017). In this study, Δt set as 1° rotation of the turbine in the same way as other researchers (Elbatran et al., 2017; Lee et al., 2016). So, it is possible to extract torque in each 1° of rotation and consequently the error is reduced. The number revolutions of the turbine were between 10 and 12 to ensure that convergence is come to pass.

4.1. Computational domain and boundary condition and grid generation

Fig. 4 displays the typical computational domain for the NPSHT. It includes two distinguished areas i.e. inner rotating area consists of SHT and the external rectangular stationary area. It is very important to have adequate interface diameter (inner area diameter) from the blades for minimizing the numerical error and assuring pressure and velocity continuity (Roy and Ducoin, 2016). Many diameters have been proposed in the literature from 1.1D to 4D (Talukdar et al., 2018; Ferrari et al., 2017; Kumar and Saini, 2017; Roy and Ducoin, 2016; Saeed et al., 2019). In the current study, the diameter of the inner region was considered 750 mm or 3D. The dimensions of the outer region were assigned 5000 mm × 3000 mm or 20D × 12D. Moving wall condition was applied for the blades. Uniform velocity was specified at the inlet, which value varies corresponds to the different Re numbers used in the study (Elbatran et al., 2017; Marsh et al., 2015). The boundary condition at the outlet was assigned as the pressure outlet. The top and bottom edges of the computational domain were considered as the symmetry boundary condition. The mentioned boundary condition has been reported as the most successful condition for predicting the performance of 2-D SHTs in several researches (Roy and Saha, 2013a; Talukdar et al., 2018; Ferrari et al., 2017; Menet, 2013; Roy and Ducoin, 2016; Tian et al., 2015; Saeed et al., 2019; Akwa et al., 2012a).

4.2. Grid generation

In a finite volume problem, grid generation with acceptable quality is essential to achieve high precision results. Accordingly, the quality of the mesh was controlled by aspect ratio and mesh

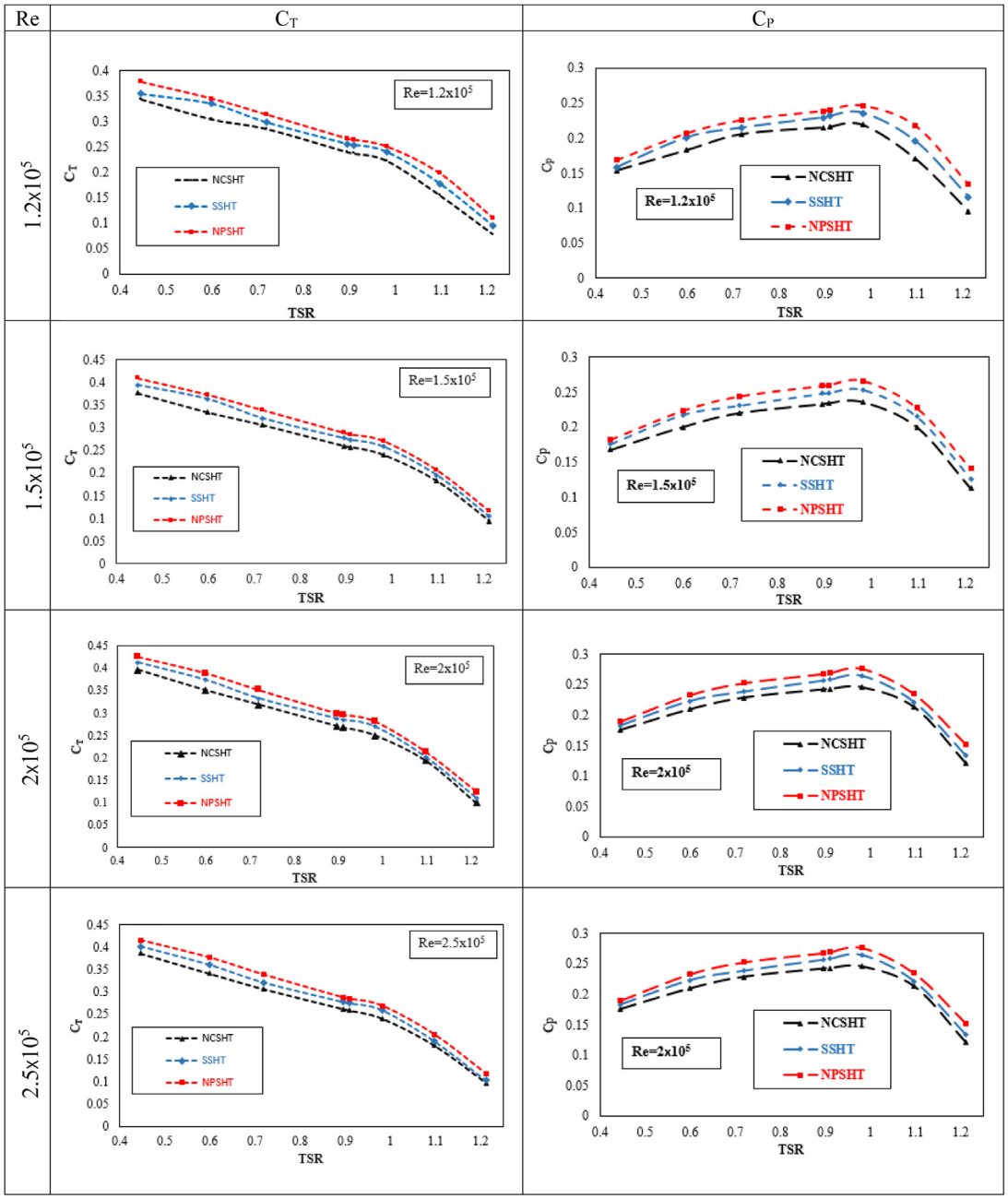

Fig. 8. Variations of C_T and C_P versus TSR at different Re numbers.

skewness. The boundary layer also plays a very important role to simulate near-wall flow and appeared adverse pressure. The boundary layer was attended by y_+ and equaled less than 1 due to the use of the SST K-ω model at different Re. The number of the boundary layer was set as 20. The structured mesh was used for the external area of the domain while for the inner rotating area triangle unstructured mesh was employed. Five different computational grids were checked to estimate the number of elements by which an independent solution can be established to obtain a converged response. This convergence study was conducted based on the obtained value of the torque coefficient (C_T) and C_P versus the number of elements. After the convergence study, the number of elements for reaching an accurate solution was obtained around 783,000 for different models. A close-up view of mesh in different regions of the computational domain is shown in Fig. 5.

5. Indicators to compute the SHTs performance

It was mentioned earlier, the main target of the present research is to analyze the performance of the NPSHT to check the efficiency enhancement as compared to its counterparts. This was implemented through realizing some performance indicators of the SHTs i.e. C_P and torque coefficient (C_T) at a different value of TSR, as presented in Eqs. (1) and (4):

$$TSR = \frac{\omega R}{V_{in}} \tag{1}$$

$$C_T = \frac{T}{0.5\rho A V_{in}^2 R} \tag{2}$$

$$C_P = \frac{P_G}{P_H} = \frac{T\omega}{0.5\rho A Vin^3} = \frac{C_T \omega R}{V_{in}} = (C_T)(TSR) \tag{3}$$

$$A = DH \tag{4}$$

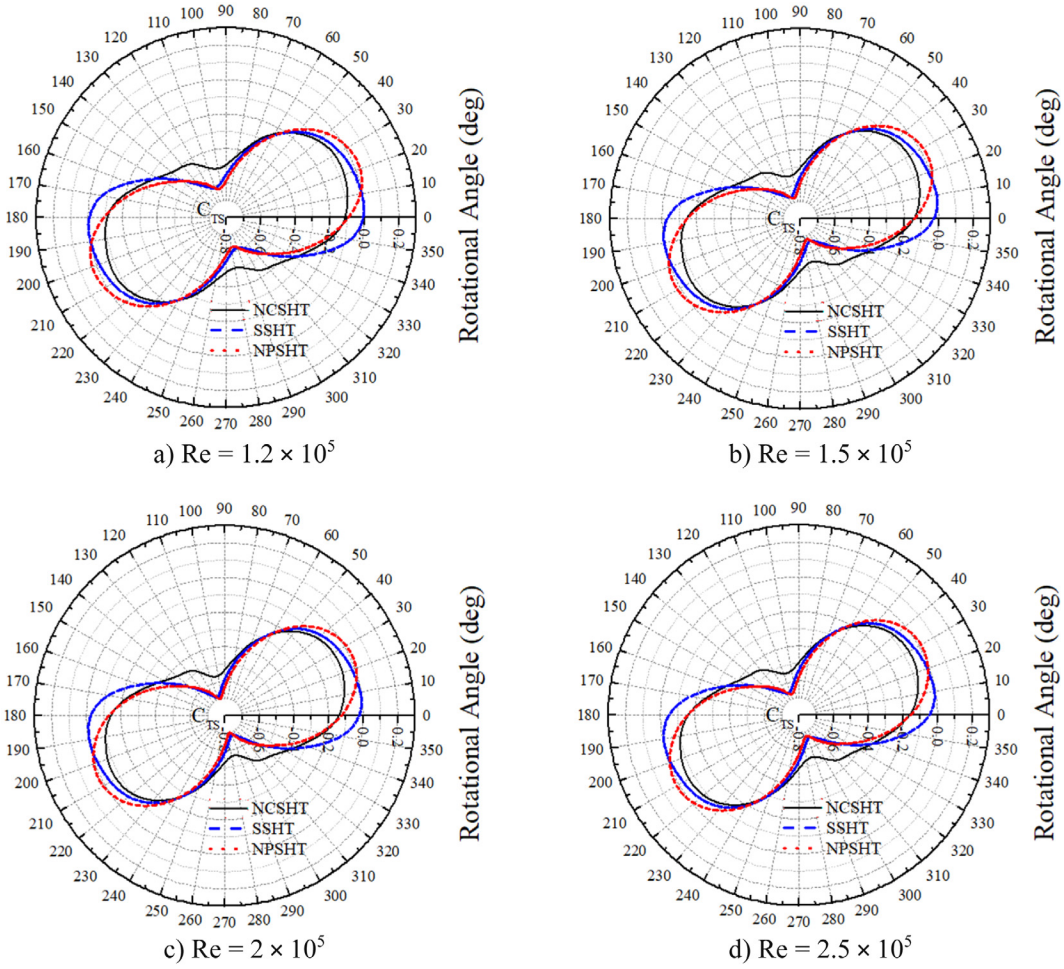

Fig. 9. Average of static torque coefficients at TSR = 0.71.

where ω is the angular velocity (rad/s), R is the radius of a turbine (m), V_{in} is the inlet velocity, P_G is the generative power of the turbine, P_H is the hydraulic energy from water, ρ is the water density, and T is the torque. A, D and H are the swept area of the turbine, turbine diameter and height of the turbine, respectively. Since in the present study, a 2-D simulation is in the process the H value was set as 1 m (Menet, 2013). Hence, the value of Re number at different flow condition can be calculated as (Talukdar et al., 2018):

$$\mathrm{Re} = \frac{\rho V_{in} D}{\mu} \tag{5}$$

where the μ is the dynamic viscosity of the fluid. In this investigation, water velocity was assumed between 0.48 and 1 m/s and so the Re values were achieved between 1.2×10^5 and 2.5×10^5. The density of water was considered 998.2 kg/m^3 and dynamic viscosity is 0.001 kg/m s^{-1}. For the validation process, the results should be compared with experimental data. Since the dimension of the presented NPSHT is similar to NCSHT (Talukdar et al., 2018), the operation condition of NCSHT (Re number = 2×10^5) was considered as a start point for the simulations. In the next steps, the up and down range of the mentioned Re number has been investigated to achieve the maximum power efficiency. In fact, the SHTs on the presented scale are more fabricated for use in the mentioned operation condition (Talukdar et al., 2018; Kumar and Saini, 2017; Roy and Ducoin, 2016; Roy and Saha, 2015).

6. Results and discussion

6.1. Validation of the developed model

The results of C_P presented in the current research for NCSHT were validated against experimental work conducted by Talukdar et al. (2018). Their experimental data on NCSHT were employed to model and validate the CFD model, since they conducted the experiments at Reynolds number equal to 2×10^5 (fall within the scope of the present work), in which the power results was extracted completely clear. To ensure the accuracy of the simulation results, different turbulence models have been examined and compared with the mentioned experimental outcomes. These comparisons are shown in Fig. 6. Results show that the SST-kω turbulence model acts nearly to the experiments as previously mentioned in Nasef et al. (2013). From Fig. 6, the root mean square error value (RMSE) between experimental and numerical data relied on using SST-kω turbulence model was around 0.026. The range of error agreed with those reported by other researchers who employed URANSE for simulations of SHTs (Talukdar et al., 2018; Ferrari et al., 2017; Roy and Ducoin, 2016; Lee et al., 2016; Dobrev and Massouh, 2011). Also, the trend of error is similar to other researches mentioned in the literature (Ferrari et al., 2017; Dobrev and Massouh, 2011) for 2-D simulation. The discrepancy of C_P results, especially in the freewheeling region, has been reported to occur due to a slight difference between the experimental and numerical values of lift and drag ratios (Ferrari et al., 2017). Thus, it can be expressed

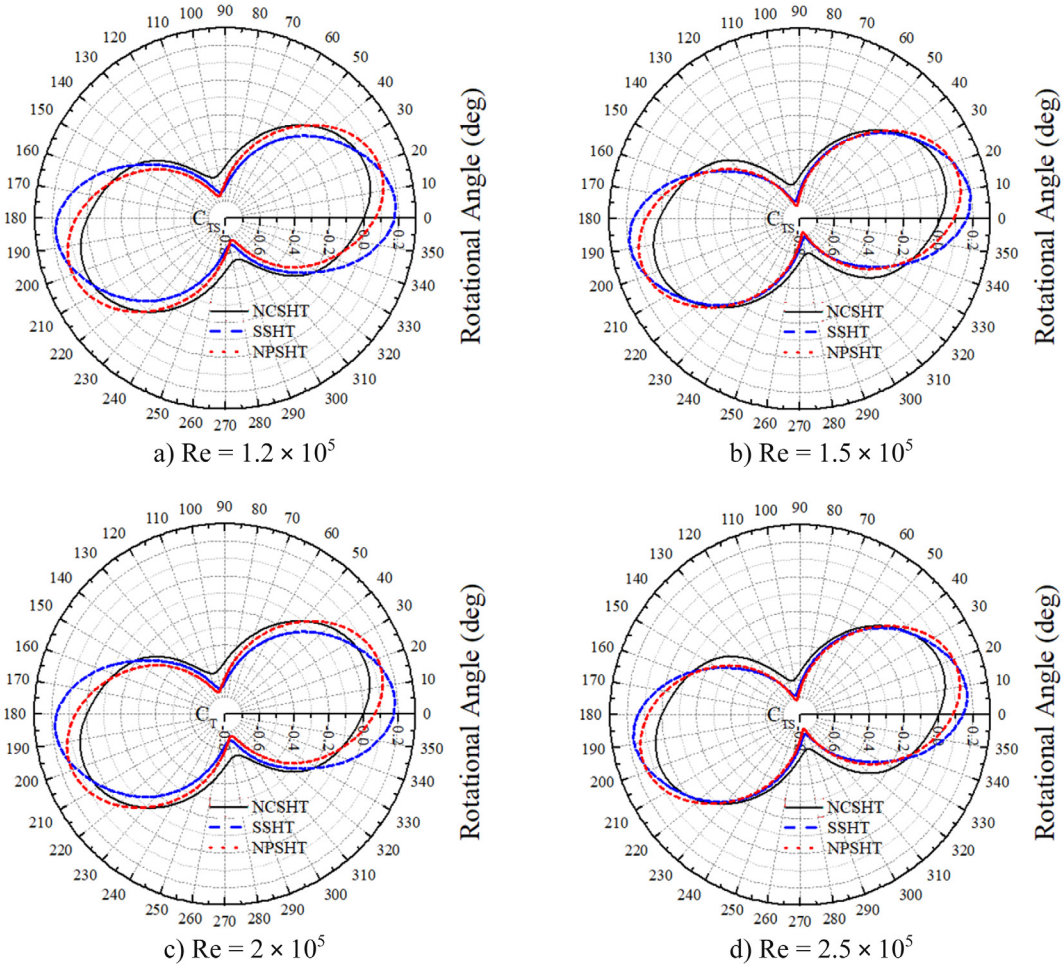

Fig. 10. Average of static torque coefficients at TSR = 0.98.

that a good agreement between CFD and experimental results was gained.

For the simulation of vertical axis turbines under unsteady flows, the time step is very important. It is suitable to set it (Δt) according to TSRs (Ferrari et al., 2017). Therefore, researchers considered district time step based on a different angle of rotation and have described Using a large time step led to unrealistic results (Kumar and Saini, 2017). In this study, to avoid this problem, different time steps from 2.5 to 0.5-degree rotation of the turbine were considered. It was found that there is no difference in outcome time steps between 1.5 and 0.5-degree rotation during meshes refinement. For each TSR, the time step is set on 10 rotation of the turbine (Elbatran et al., 2017; Lee et al., 2016). Therefore, it is possible to extract torque for every 10 rotations and reduce the computational error. (see Fig. 7).

6.2. Dynamic performance

This section provided a comparative study to assess the performance of all three models discussed in this research. Fig. 8 shows that for all models, the variations trend of C_T versus TSR at all values of Re numbers in the range ($1.2 \times 10^5 \leq Re \leq 2.5 \times 10^5$) were the same. A similar trend can be also observed for C_p. Thus, it can be expressed that, the C_T extracted from a SHT independent form its type, has a significant effect on the C_P.

From Fig. 8, it can be revealed that for all models, the C_T values decrease with the increase of TSR. Previous researchers (Roy and Saha, 2015) attribute this phenomenon to the gradual loads exerted to the SHT rotor, which in turn, reduces the turbine angular velocity. On the other hand, the C_P enhances with an increase of TSR up to a C_{Pmax}, then after, it declines at higher values of TSR. Also, it is observed that the C_T increases with an increase of Re number up to a certain maximum value i.e. 2×10^5 due to an increase of generated momentum. Beyond such Re number, C_T decreases because an increase in vortices comes in to play. So, for all three models, the maximum amount of C_T occurred at Re number 2×10^5 which is more than that of Re numbers 2.5×10^5, 1.5×10^5, and 1.2×10^5, respectively. Thus, the Re number 2×10^5 may be nominated as the optimal value for torque generation. It is completely clear that, at all Re numbers, the C_T of the NPSHT is higher than that of SSHT and NCSHT, severally.

Similarly, Fig. 8 demonstrates that NPSHT shows an improvement in C_{Pmax} as compared to other simulated turbines. The C_{Pmax} for all SHTs occurred at $Re = 2 \times 10^5$. This value was 0.25, 0.26, 0.28 for NCSHT, SSHT, and NPSHT, respectively. In fact, the C_{Pmax} gains of the NPSHT over SSHT and NCSHT was found to be 7.7% and 12%, severally. The recent trend was similar for all values of Re numbers. It is worth noting that NPSHT is located firmly in the highest amount of C_{Pmax} at different Re numbers. Also, it should be noted that the C_{Pmax} for all cases and at all Re numbers has been situated at TSR 0.98. Likewise, obtaining C_{Pmax} at different Re numbers but the same value of TSR has been previously reported by Kumar and Saini (2017) that was observed at TSR 0.9.

6.3. Static performance

The average of static torque (C_{Ts}) for each revolution leads to determine the overall C_T and subsequently computing Cp.

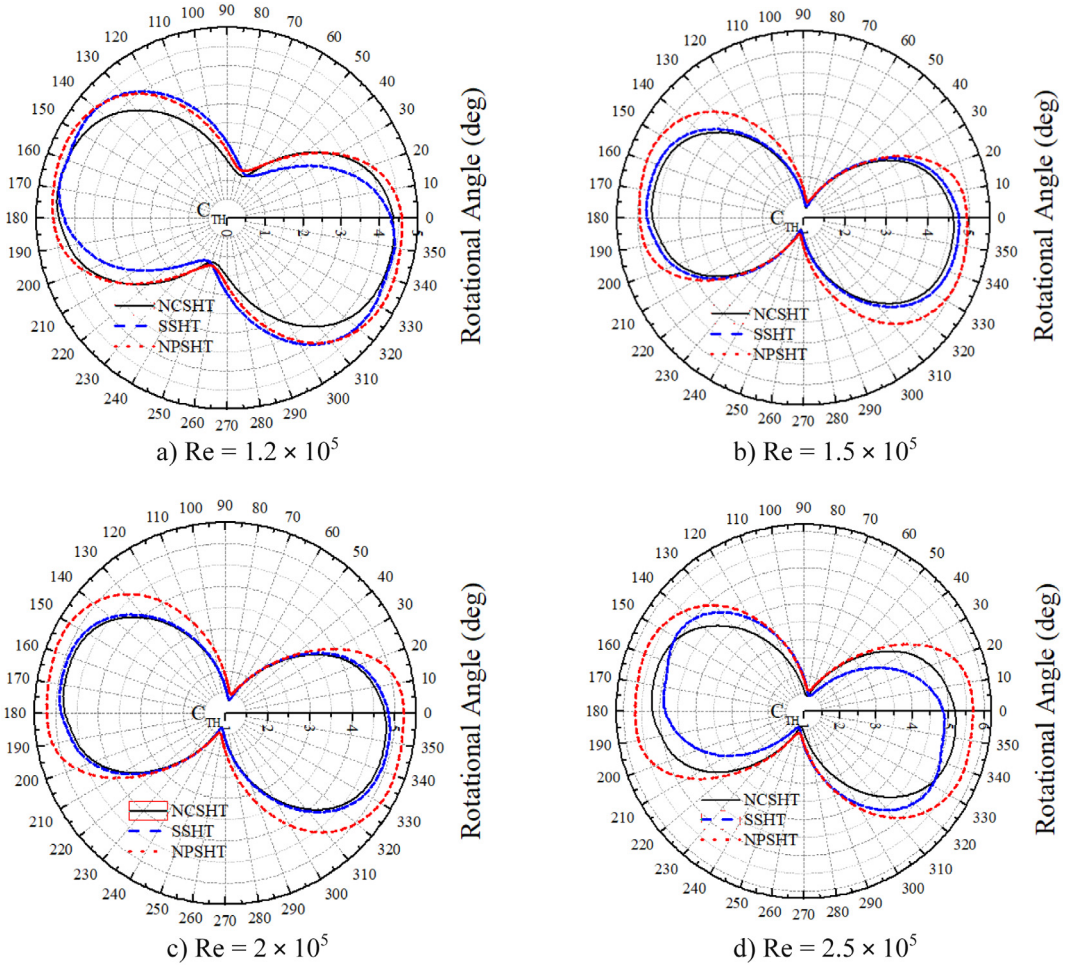

Fig. 11. Thrust coefficients at TSR = 0.71.

It is worth mentioning that to demonstrate the performance discrepancy among all three models presented in this research, 96 simulations were needed to be run. Since presenting all the results in the paper was not possible, just a couple of TSRs were selected. Figs. 9 and 10 display the variation of C_{Ts} versus rotational angle at TSRs 0.71 and 0.98 for different Re numbers. Also, Figs. 11 and 12 show the variation of C_{TH} versus rotational angle at the same conditions. From Fig. 9, it is clear that for Re numbers between 1.2×10^5 and 2.5×10^5 at TSR = 0.71, the SSHT obtains a lower C_{TS} in the range of rotational angle between 150° to 185°. At the same condition, NPSHT shows a nearly similar performance to the NCSHT, but it gains more C_{TS}. In this situation, C_{Ts} is a function of C_{TH} which can be considered as a significant parameter to increase or decrease C_{TS}. On the other hand, from Figs. 9 and 11, considering rotational angle in the range of 80° to 105°, it is realized that, NCSHT is suffering from low generated torque as compared to SSHT and NPSHT due to low C_{TH}. In this angular position, SSHT and NPSHT perform closely however, NPSHT has again better efficacy as compared to SSHT.

From Figs. 10 and 12, it can be revealed that for Re numbers 1.2×10^5 to 2.5×10^5 at TSR = 0.98 the maximum value of C_{TS} has been obtained in the range of rotational angle between 85° to 125° for all three models while the amount of C_{TH} decreased. This thrust drop is related to the reduction of the cross-sectional area of the turbine that is exposed to the flow at this rotational angle range. However, in this situation, more lift occurs and the thrust acting on the returning blade decreases and consequently the amount of C_{TS} increases. Figs. 10 and 12 also show, under the same condition, NCSHT has been still remained at the lowest C_{TS} while SSHT & NPSHT have more capability to generate C_{TS}. In fact, for NCSHT, lower thrust is applied to advancing blade and lower lift generates. In this case, better performance can be observed for NPSHT as compared to SSHT. In general, the maximum C_{TS} of the NPSHT is 4% higher than that of the SSHT and 25.8% than that of the NCSHT.

From Figs. 9 and 10, a fluctuation in the extracted torque can be detected. This fluctuation may attribute to the torque changes on the advancing and returning blades from positive to negative and vice versa. Considering Fig. 9, the most fluctuation of the torque is observed in the range of 50° to 150° for TSR = 0.71. This *fluctuation* leads to hold NCSHT at its maximum torque extraction for a longer period. Nonetheless, its C_{TS} is lower than that of SSHT and NPSHT and thus the NCSHT performance decreases. From Fig. 10, for TSR = 0.98 the most fluctuation of the C_{TS} is observed in the range of 140° to 200°. Under this situation, the fluctuation of CTS for NCSHT is more than that of SSHT and NPSHT however, it is oriented to avoid negative C_{TS} and leads to increase its performance in comparison with SSHT and NPSHT. Similarly, the fluctuation of C_{TS} for SSHT is more than that of NPSHT nevertheless, it causes C_{TS} is not fallen within the negative area and as the result, its performance enhances.

Although the study of the dynamic and static performances of SHTs are able to explain the relationship between the turbine geometry and generated thrust, torque and power, however

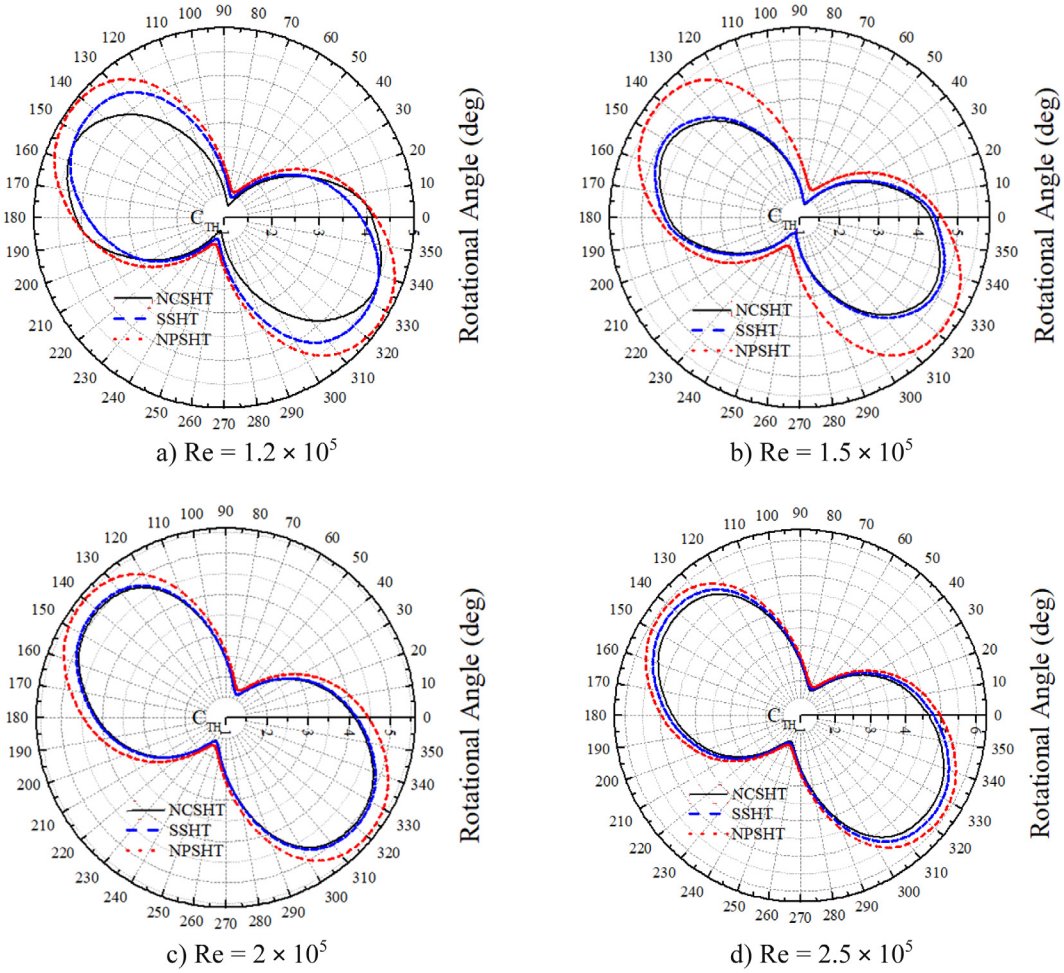

Fig. 12. Thrust coefficients at TSR = 0.98.

they are not an appropriate criterion to interpret all parameters contributing to the issue of performance in different situations. Therefore, further discussion through plotting pressure and velocity contours need to be presented.

6.4. Pressure contours

As per mentioned, SHTs operate based on the drag force so that the pressure drops between the concave side of the advancing blade and the convex side of the returning blade influences the turbine rotation. So, it is necessary to analyze the pressure contours for obtaining an in-depth understanding of SHTs performance. Figs. 13 and 14 show the pressure contours for all three models presented in this study in the different operational situations. Form these figures, it can be realized, at the condition including Re number 1.2×10^5, TSR 0.71 and rotational angle 165°, the effective area of pressure zone for the concave side of the advancing blade in NCSHT and NPSHT is more than that of SSHT, but increasing in overlap ratio and torque arm from the center of rotation to center of pressure lead to generate more torque in NPSHT. Similarly, it occurs for the other situations e.g. Re $= 2 \times 10^5$ (TSR = 0.71, rotational angle = 165°), Re $= 2.5 \times 10^5$ (TSR = 0.71, rotational angle = 180°), and Re $= 2.5 \times 10^5$ (TSR = 0. 98, rotational angle = 90°).

At Re $= 1.2 \times 10^5$ (TSR = 0.98, rotational angle = 120°) and Re $= 1.5 \times 10^5$ (TSR = 0.71, rotational angle = 90°), considering the high pressure value on the concave side of advancing blades, it is clear that pressure drag increases for SSHT and NPSHT. Also, the torque arm is observed to be higher for SSHT and NPSHT than that of NCSHT and as the result, the torque increases. On the other hand, observing the pressure contours in this situation (Fig. 10), it can be considered that the maximum positive pressure (red contours) disappears on the way of the convex side of the returning blade for NPSHT as compared to SSHT, so the negative torque reduces and performance increases. This phenomenon was occurred at Re $= 2 \times 10^5$ (TSR = 0.98, rotational angle = 105°), and Re $= 2.5 \times 10^5$ (TSR = 0.98, rotational angle = 90°). Likewise, by observing the pressure contours, it is clear that the increase of Re number leads to an increase in the pressure drop between the concave side of the advancing blade and the convex side of returning blades.

6.5. Velocity contours

In order to achieve the physical reasons behind the performance improvement of the NPSHT over NCSHT and SSHT, the flow velocity contours around all three models need to be plotted. Figs. 15 and 16 show the velocity contours for the Re numbers in the range of 1.2×10^5 to 2.5×10^5. From these figures, it can be found the water velocity at the inlet is constant up to the inner area including SHT. When SHTs rotate, two separate areas i.e. a high velocity region near the tip of the blades and low velocity or wake region at the downstream of the SHT appear. It has been previously reported in Talukdar et al. (2018), Kumar and Saini (2017) and Ostos et al. (2019). At TSR = 0.71 and for (Re $= 1.2 \times 10^5$, rotational angle = 165°), (Re $= 2 \times 10^5$, rotational angle =

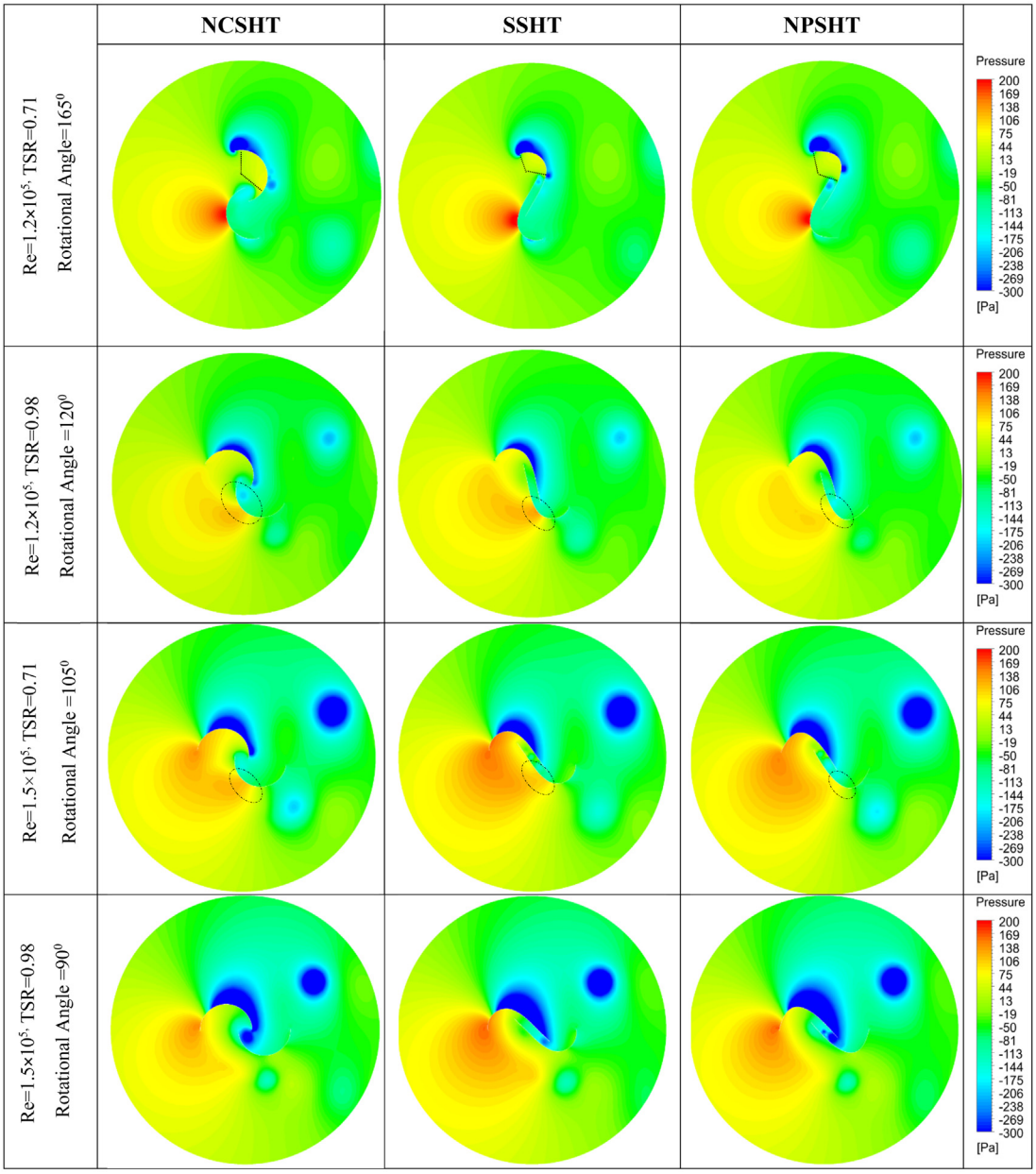

Fig. 13. Pressure contours at Re numbers 1.2×10^5 and 1.5×10^5.

165°), and (Re = 2.5×10^5, rotational angle = 165°), high speed vortices are observed near the tip of advancing blade regions that causes to generate a low pressure zone in such regions. This pattern leads the flow moves with high velocity and passes from the turbines so that far less exchange in the momentum between the flowstream and SHT occurs and consequently the torque reduces. Also, it sounds that increasing the Re number is mainly responsible for generation the high speed vortices around the leading edge which causes to reduce the torque in such area.

At TSR 0.98 and (Re = 1.2×10^5, rotational angle = 120°), (Re = 1.5×10^5, rotational angle = 90°), (Re = 2×10^5, rotational angle = 105°) and (Re = 2.5×10^5, rotational angle = 90°), it is realized that the advancing blade of NPSHT is subjected to higher velocity gradient as compared to the SSHT and NCSHT. It may attribute to the parabolic blade shape of NPSHT that is capable to create more surface area on the way of the flow. Therefore, an increase in the velocity gradient results in more power output and C_T. This change in geometry also leads to an increase in the torque arm from the center of rotation to the center of lift which boosts the NPSHT performance. According to the mentioned, SSHT and NCSHT are placed in the next ranks, respectively. The same results but in the case of SWTs can be observed in Roy and Ducoin (2016).

6.6. Performance comparison with counterparts

Some of the reported results in the case of 2-bladed SHT have been tabulated in Table 2. It is worth mentioning that all of the researches listed in this table are on the performance of SHTs in the water flow. As it can be observed, the computational evaluations implemented by Roy and Ducoin (2016), Roy and Saha (2015) and also the present study indicate that at the same condition, the SHTs with arc shaped followed by a straight arc blade show more acceptable performance than the semicircular blade SHTs. However, the present study shows a parabolic blade SHT obtains a higher C_{Pmax} in comparison to semicircular (Talukdar et al., 2018) and arc shaped followed by a straight arc bladed SHT (Roy and Ducoin, 2016; Roy and Saha, 2015) at the analogous situation. Further, comparing the results presented in the Talukdar

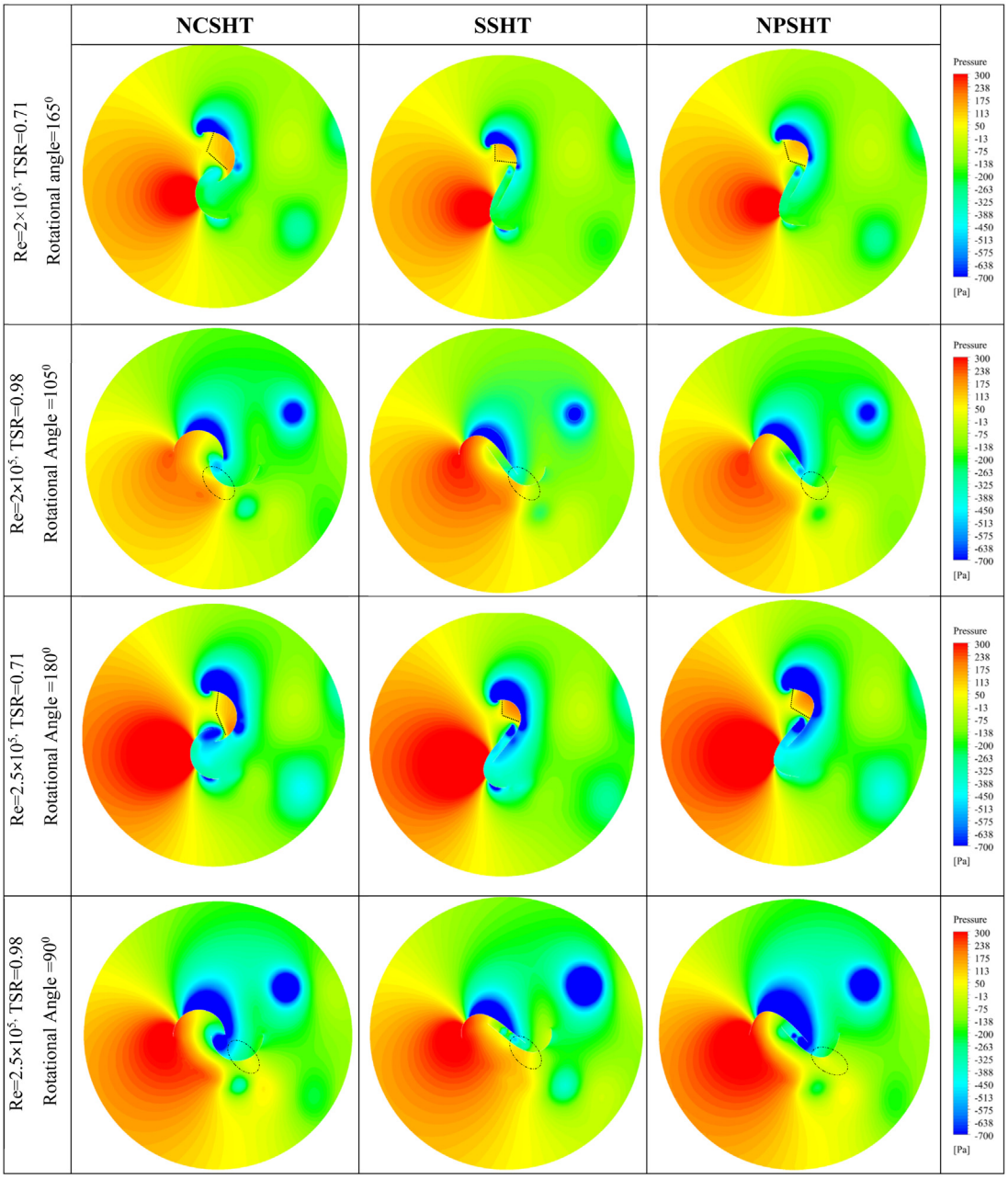

Fig. 14. Pressure contours at Re numbers 2×10^5 and 2.5×10^5.

et al. (2018) with Elbatran et al. (2017) reveals that changing the blade geometry from semicircular to the arc shaped followed by a straight arc (partially straight blade) leads to achieve an equivalent C_{Pmax}, but at lower TSR and Re number.

For better comparison and understanding, the computational results presented in Table 2 are shown in Fig. 17. By referring to Table 2 and Fig. 16, concerning the C_{Pmax}, it is obvious that NPSHT is advantageous over the SSHT, NCSHT, S2, S3 and S4. It can be attributed to its parabolic geometry in which, an increase of overlap ratio and torque arm from the center of rotation to the center of pressure lead to generate more torque as compared to the other geometry. Moreover, this change in geometry and subsequently providing more surface area along the way of flow causes the advancing blade of NPSHT is subjected to higher velocity gradient and lift increases so that more C_P can be achieved. Hence, the C_{Pmax} of the NPSHT is 7.7%, 12%, 12%, 12% and 100% higher than that of the SSHT, NCSHT, S2, S3 and S4, respectively.

On the other hand, from Fig. 17 and Table 2, it can be observed that as a geometry of NPSHT changes to S1, its C_{Pmax} increases at around 28%. This discrepancy between these two results may due to the twisted blade shape of S1. Though this type of blade may increase the C_{Pmax} however, its geometrical complexity makes the manufacturing process costly, time-consuming and cumbersome as compared to the NPSHT. From the other point of view, when browsing Table 2, the S1 showing the C_{Pmax} at $Re = 3.95 \times 10^5$. Nevertheless, in our present study, the NPSHT obtained C_{Pmax} at $Re = 2 \times 10^5$ which is far less than that of S1. Identically, this higher Re number has a significant effect on the extracted torque and power of the turbine. Plus, a more complex and expensive gearbox for controlling the rotational movement of S1 is required. Therefore, a further extensive parametric study on these two types of SHT in the same flow conditions has to be conducted.

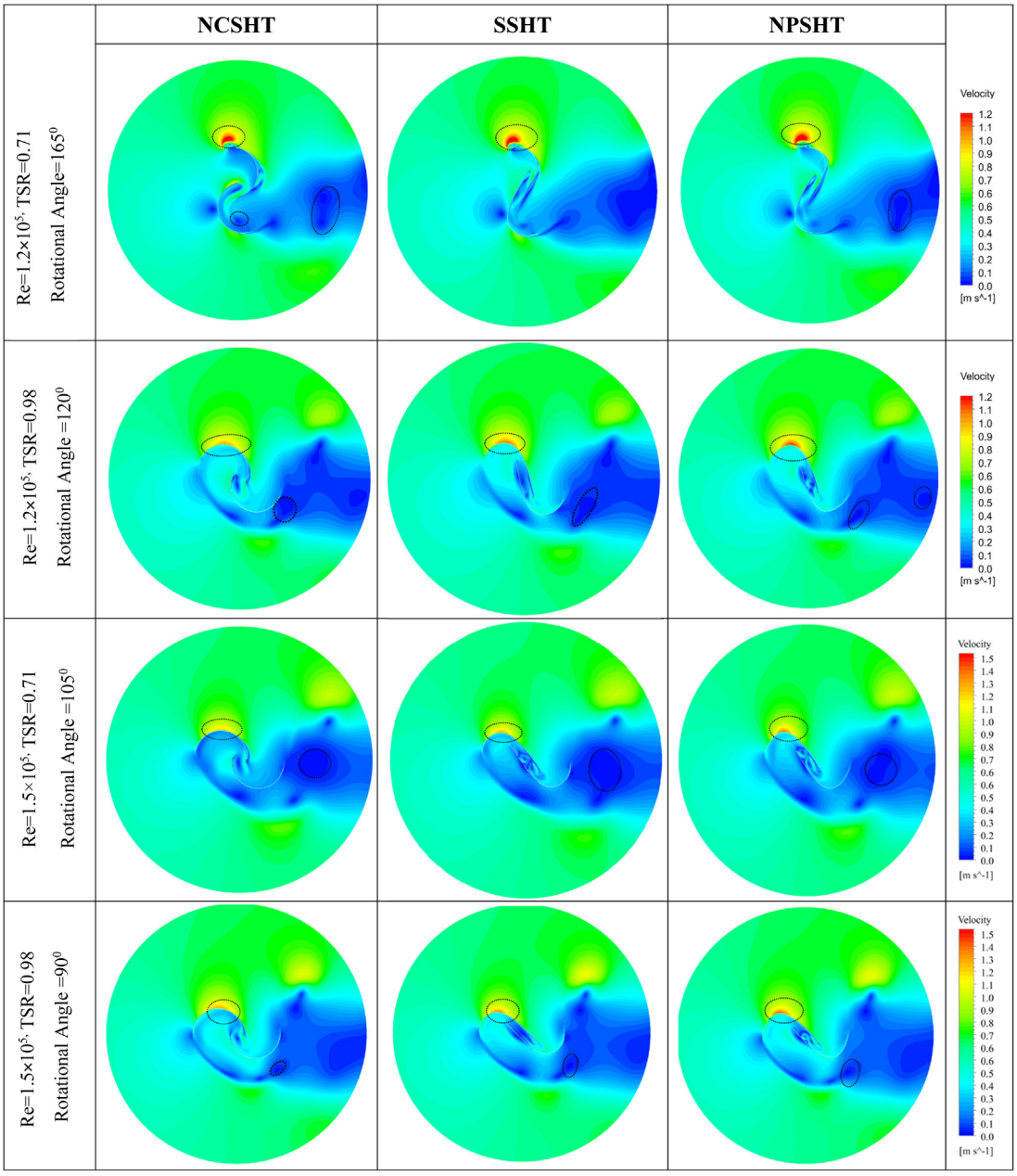

Fig. 15. Velocity contours at Re numbers 1.2×10^5 and 1.5×10^5.

Table 2
Some reported studies on SHTs.

Reference	Code	Blade shape	D (mm)	e (mm)	A_d (mm)	AR	TSR	Re	C_{Pmax}
Kumar and Saini (2017)	S1	Twisted blade	160	0	0	1.6	0.90	3.59×10^5	0.39
Present study	NPSHT	Parabolic	250	82.50	35.00	1.0	0.98	2×10^5	0.28
Roy and Ducoin (2016) and Roy and Saha (2015)	SSHT	Arc shaped followed by a straight arc	250	37.50	30.00	1.0	0.98	2×10^5	0.26
Talukdar et al. (2018)	NCSHT	Semicircular	250	112.50	37.50	1.0	0.98	2×10^5	0.25
Nakajima et al. (2008)	S2	Semicircular	142	51.12	51.12	–	1.100	1.1×10^5	0.25
Elbatran et al. (2017)	S3	Arc shaped followed by a straight arc	245	–	–	0.7	0.73	1.32×10^5	0.25
Kailash et al. (2012)	S4	Circular arc followed by a straight arc	245	–	–	0.7	0.70	1.32×10^5	0.14

7. Conclusions

In this paper, the performance of a new proposed hydrokinetic Savonius turbine was investigated through a computational fluid dynamic analysis and results were compared and discussed with Savonius style hydrokinetic turbine and new conventional Savonius hydrokinetic turbine; both presented in the literature. The main observations are summarized as follows

(a) With develop the new proposed hydrokinetic Savonius turbine, a remarkable improvement in the C_{Pmax} was obtained

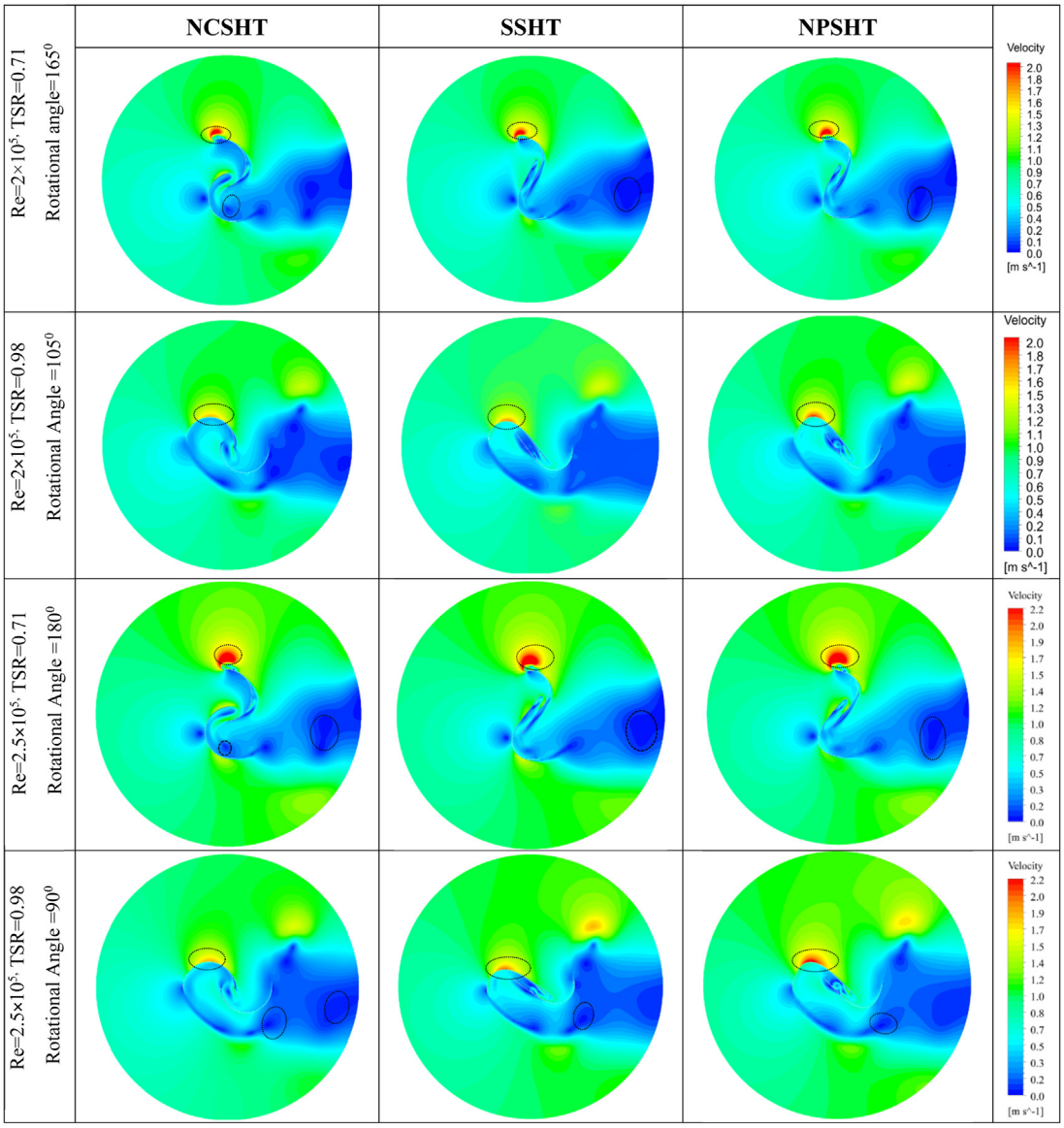

Fig. 16. Velocity contours at Re numbers 2×10^5 and 2.5×10^5.

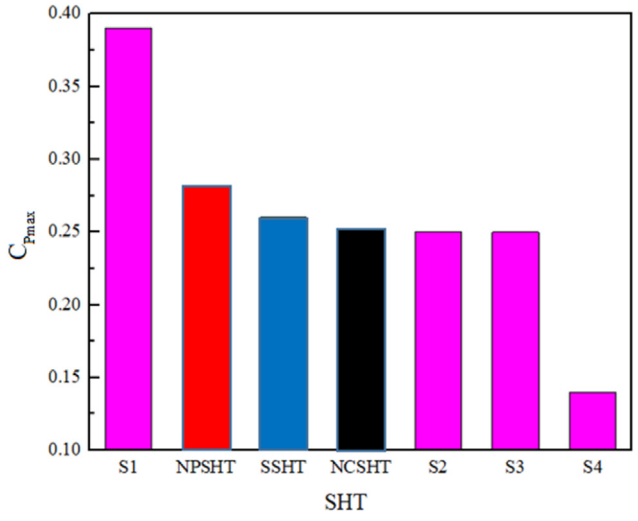

Fig. 17. C_{Pmax} of NPSHT as compared to some SHTs reported in the literature.

over other models presented previously. Performance gains of 7.7% and 12% were achieved over Savonius style hydrokinetic turbine and new conventional Savonius hydrokinetic turbine, respectively.

(b) The new proposed hydrokinetic Savonius turbine can increase the value of the C_{TS}, so that the maximum value of C_{TS} of the new proposed hydrokinetic Savonius turbine is higher by 4% and 25.8% than the Savonius style hydrokinetic turbine and new conventional Savonius hydrokinetic turbine, respectively.

(c) The new proposed hydrokinetic Savonius turbine not only could reduce the positive pressure on the returning blade at some district rotational angle, but also increased the lift of the advancing blade to some extent due to switching the blade geometry into the parabolic shape.

(d) With the increase of Reynolds number, the dynamic performance indicators i.e. the C_P and C_T and the static performance indicator i.e. C_{TS} and C_{TH} enhanced up to a certain limit of Reynolds number $= 2 \times 10^5$, beyond which it again declined.

(e) For all three simulated blade profiles, the C_{Pmax} values were experienced at an optimum value of tip speed ratio 0.98

and Reynolds number 2×10^5. However, the new proposed hydrokinetic Savonius turbine at all Reynolds numbers and tip speed ratios in the scope of this research showed better performance than the other simulated models.

(f) In general, the parabolic geometry was able to gain better performance as compared to its counterparts. This was mainly due to provide an effective area of high pressure drag on the advancing blade assisting with an increase of the torque arm from the center of rotation to both centers of pressure and lift.

This study focused on the performance of small-scale NPSHT where a single turbine is utilized. Investigation of the concept of employing vertical arrays of small-scale NPSHTs substituted for a single large NPSHT can further be implemented in the future works.

CRediT authorship contribution statement

Ramin Alipour: Conception and design of study, Acquisition of data, Analysis and/or interpretation of data, Writing - original draft, Writing - review & editing. **Roozbeh Alipour:** Conception and design of study, Acquisition of data, Analysis and/or interpretation of data, Writing - original draft, Writing - review & editing. **Farhad Fardian:** Conception and design of study, Acquisition of data, Analysis and/or interpretation of data, Writing - review & editing. **Seyed Saeid Rahimian Koloor:** Conception and design of study, Writing - review & editing. **Michal Petrů:** Conception and design of study, Writing - review & editing.

Declaration of competing interest

The authors declare that they have no known competing financial interests or personal relationships that could have appeared to influence the work reported in this paper.

Acknowledgments

The research was supported by the Ministry of Education, Youth, and Sports of the Czech Republic and the European Union (European Structural and Investment Funds Operational Program Research, Development, and Education) in the framework of the project "Modular platform for autonomous chassis of specialized electric vehicles for freight and equipment transportation", Reg. No. CZ.02.1.01/0.0/0.0/16_025/0007293, as well as the financial support from internal grants in the Institute for Nanomaterials, Advanced Technologies and Innovations (CXI), Technical University of Liberec (TUL). All authors approved the version of the manuscript to be published.

References

Abraham, J., et al., 2011. Numerical simulation of fluid flow around a vertical-axis turbine. J. Renew. Sustain. Energy 3 (3), 033109.

Afungchui, D., et al., 2010. The unsteady pressure field and the aerodynamic performances of a savonius rotor based on the discrete vortex method. Renew. Energy 35 (1), 307–313.

Akwa, J.V., da Silva Júnior, G.A., Petry, A.P., 2012a. Discussion on the verification of the overlap ratio influence on performance coefficients of a Savonius wind rotor using computational fluid dynamics. Renew. Energy 38 (1), 141–149.

Akwa, J.V., Vielmo, H.A., Petry, A.P., 2012b. A review on the performance of savonius wind turbines. Renew. Sustain. Energy Rev. 16 (5), 3054–3064.

Al-Dabbagh, M.A., Yuce, M.I., 2018. Simulation and comparison of helical and straight-bladed hydrokinetic turbines. Int. J. Renew. Energy Res. 8 (1), 504–513.

Alipour, R., 2011. Finite element analysis of elongation in free explosive forming of aluminum alloy blanks using CEL method. Int. Rev. Mech. Eng. 5 (6), 1039–1042.

Alipour, R., Farokhi Nejad, A., Nilsaz Dezfouli, H., 2018. Steady state creep characteristics of a ferritic steel at elevated temperature: An experimental and numerical study. ADMT J. 11 (4), 115–129.

Alipour, R., Najarian, F., 2011. A FEM study of explosive welding of double layer tubes. World Acad. Sci., Eng. Technol. 73, 954–956.

Alipour, R., Nejad, A.F., 2016. Creep behaviour characterisation of a ferritic steel alloy based on the modified theta-projection data at an elevated temperature. Int. J. Mater. Res. 107 (5), 406–412.

Alipour, R., et al., 2009. Explosive welding simulation of double layer tubes (7039 Aluminium-4340 steel). in: NMEC02. 2009. Najafabad, Isfahan, Iran.

Alipour, R., et al., 2020. On the performance of small-scale horizontal axis tidal current turbines. Part 1: One single turbine. Sustainability 12 (15), 5985.

Alom, N., et al., 2016. Aerodynamic design optimization of elliptical-bladed savonius-style wind turbine by numerical simulations. In: ASME 2016 35th International Conference on Ocean, Offshore and Arctic Engineering. American Society of Mechanical Engineers Digital Collection.

Altan, B.D., Atılgan, M., 2008. An experimental and numerical study on the improvement of the performance of Savonius wind rotor. Energy Convers. Manage. 49 (12), 3425–3432.

Antheaume, S., Maître, T., Achard, J.-L., 2008. Hydraulic darrieus turbines efficiency for free fluid flow conditions versus power farms conditions. Renew. Energy 33 (10), 2186–2198.

Banerjee, A., et al., 2014. Unsteady flow analysis around an elliptic-bladed savonius-style wind turbine. In: ASME 2014 Gas Turbine India Conference. American Society of Mechanical Engineers Digital Collection.

Benesh, A.H., 1996. Wind turbine with savonius-type rotor. Google Patents.

Chatzirodou, A., Karunarathna, H., Reeve, D.E., 2019. 3D modelling of the impacts of in-stream horizontal-axis tidal energy converters (TECs) on offshore sandbank dynamics. Appl. Ocean Res. 91, 101882.

Dobrev, I., Massouh, F., 2011. CFD and PIV investigation of unsteady flow through Savonius wind turbine. Energy Procedia 6, 711–720.

Elbatran, A., Ahmed, Y.M., Shehata, A.S., 2017. Performance study of ducted nozzle Savonius water turbine, comparison with conventional savonius turbine. Energy 134, 566–584.

Emmanuel, B., Jun, W., 2011. Numerical study of a six-bladed savonius wind turbine. J. Solar Energy Eng. 133 (4).

Faizal, M., Ahmed, M.R., Lee, Y.-H., 2010. On utilizing the orbital motion in water waves to drive a savonius rotor. Renew. Energy 35 (1), 164–169.

Ferrari, G., et al., 2017. CFD study of savonius wind turbine: 3D model validation and parametric analysis. Renew. Energy 105, 722–734.

Fujisawa, N., Gotoh, F., 1994. Experimental study on the aerodynamic performance of a savonius rotor.

Golecha, K., Eldho, T., Prabhu, S., 2011. Influence of the deflector plate on the performance of modified Savonius water turbine. Appl. Energy 88 (9), 3207–3217.

Gorlov, A., 1998. Development of the Helical Reaction Hydraulic Turbine. Final Technical Report, Northeastern Univ., Boston, MA (United States).

Han, D., et al., 2018. Design, fabrication, and performance test of a 100-w helical-blade vertical-axis wind turbine at low tip-speed ratio. Energies 11 (6), 1517.

Kailash, G., Eldho, T., Prabhu, S., 2012. Performance study of modified savonius water turbine with two deflector plates. Int. J. Rotating Mach. 2012.

Kamoji, M., Kedare, S.B., Prabhu, S., 2009. Experimental investigations on single stage modified savonius rotor. Appl. Energy 86 (7–8), 1064–1073.

Khan, M., et al., 2009a. Hydrokinetic energy conversion systems and assessment of horizontal and vertical axis turbines for river and tidal applications: A technology status review. Appl. Energy 86 (10), 1823–1835.

Khan, M., et al., 2009b. Performance of savonius rotor as a water current turbine. J. Ocean Technol. 4 (2), 71–83.

Kumar, A., Saini, R., 2016. Performance parameters of savonius type hydrokinetic turbine–A review. Renew. Sustain. Energy Rev. 64, 289–310.

Kumar, A., Saini, R., 2017. Performance analysis of a savonius hydrokinetic turbine having twisted blades. Renew. Energy 108, 502–522.

Lanzafame, R., Mauro, S., Messina, M., 2014. 2D CFD modeling of h-darrieus wind turbines using a transition turbulence model. Energy Procedia 45, 131–140.

Lee, J.-H., Lee, Y.-T., Lim, H.-C., 2016. Effect of twist angle on the performance of savonius wind turbine. Renew. Energy 89, 231–244.

Liu, J., et al., 2017. The effects of blade twist and nacelle shape on the performance of horizontal axis tidal current turbines. Appl. Ocean Res. 64, 58–69.

Mahmoud, N., et al., 2012. An experimental study on improvement of savonius rotor performance. Alexandria Eng. J. 51 (1), 19–25.

Mari, M., Venturini, M., Beyene, A., 2017. A novel geometry for vertical axis wind turbines based on the savonius concept. J. Energy Resour. Technol. 139 (6), 061202.

Marsh, P., et al., 2015. Three-dimensional numerical simulations of straight-bladed vertical axis tidal turbines investigating power output, torque ripple and mounting forces. Renew. Energy 83, 67–77.

Menet, J.-L., 2013. Static and dynamic study of a conventional savonius rotor using a numerical simulation/Étude statique et dynamique dún rotor Savonius conventionnel par simulation numérique. In: Congrès Français de Mécanique. AFM, Maison de la Mécanique, 39/41 rue Louis Blanc, 92400 Courbevoie, France....

Menter, F.R., 1994. Two-equation eddy-viscosity turbulence models for engineering applications. AIAA J. 32 (8), 1598–1605.

Mercier, P., et al., 2020. Numerical study of the turbulent eddies generated by the seabed roughness. Case study at a tidal power site. Appl. Ocean Res. 97, 102082.

Michelet, N., et al., 2020. Three-dimensional modelling of turbine wake interactions at a tidal stream energy site. Appl. Ocean Res. 95, 102009.

Mohamed, M., et al., 2010. Optimization of savonius turbines using an obstacle shielding the returning blade. Renew. Energy 35 (11), 2618–2626.

Najarian, F., et al., 2019. Hole quality assessment in drilling process of basalt/epoxy composite laminate subjected to the magnetic field. Mech. Ind. 20 (6), 620.

Nakajima, M., Iio, S., Ikeda, T., 2008. Performance of savonius rotor for environmentally friendly hydraulic turbine. J. Fluid Sci. Technol. 3 (3), 420–429.

Nasef, M., et al., 2013. Evaluation of savonius rotor performance: Static and dynamic studies. J. Wind Eng. Ind. Aerodyn. 123, 1–11.

Ostos, I., et al., 2019. A modified novel blade configuration proposal for a more efficient VAWT using CFD tools. Energy Convers. Manage. 180, 733–746.

Owusu, P.A., Asumadu-Sarkodie, S., 2016. A review of renewable energy sources, sustainability issues and climate change mitigation. Cogent Eng. 3 (1), 116799.

Patel, V., et al., 2017. Influence of overlap ratio and aspect ratio on the performance of savonius hydrokinetic turbine. Int. J. Energy Res. 41 (6), 829–844.

Ramar, S.K., Seralathan, S., Hariram, V., 2018. Numerical analysis of different blade shapes of a savonius style vertical axis wind turbine. Int. J. Renew. Energy Res. (IJRER) 8 (3), 1657–1666.

Rogowski, K., Maroński, R., 2015. CFD computation of the savonius rotor. J. Theoret. Appl. Mech. 53 (1), 37–45.

Rossetti, A., Pavesi, G., 2013. Comparison of different numerical approaches to the study of the h-darrieus turbines start-up. Renew. Energy 50, 7–19.

Roy, S., 2014. Aerodynamic performance evaluation of a novel savonius0style wind turbine through unsteady simulations and wind tunnel experiments.

Roy, S., Ducoin, A., 2016. Unsteady analysis on the instantaneous forces and moment arms acting on a novel Savonius-style wind turbine. Energy Convers. Manage. 121, 281–296.

Roy, S., Saha, U.K., 2013a. Numerical investigation to assess an optimal blade profile for the drag based vertical axis wind turbine. In: ASME 2013 International Mechanical Engineering Congress and Exposition. American Society of Mechanical Engineers Digital Collection.

Roy, S., Saha, U.K., 2013b. Review of experimental investigations into the design, performance and optimization of the savonius rotor. Proc. Inst. Mech. Eng., Part A 227 (4), 528–542.

Roy, S., Saha, U.K., 2013c. Review on the numerical investigations into the design and development of savonius wind rotors. Renew. Sustain. Energy Rev. 24, 73–83.

Roy, S., Saha, U.K., 2014. An adapted blockage factor correlation approach in wind tunnel experiments of a savonius-style wind turbine. Energy Convers. Manage. 86, 418–427.

Roy, S., Saha, U.K., 2015. Wind tunnel experiments of a newly developed two-bladed Savonius-style wind turbine. Appl. Energy 137, 117–125.

Saeed, H.A.H., Elmekawy, A.M.N., Kassab, S.Z., 2019. Numerical study of improving savonius turbine power coefficient by various blade shapes. Alexandria Eng. J..

Sarma, N., Biswas, A., Misra, R., 2014. Experimental and computational evaluation of savonius hydrokinetic turbine for low velocity condition with comparison to savonius wind turbine at the same input power. Energy Convers. Manage. 83, 88–98.

Sawin, J.L., et al., 2018. Renewables 2018. Global Status Report 2018.

Sivasegaram, S., 1978. Secondary parameters affecting the performance of resistance-type vertical-axis wind rotors. Wind Eng. 49–58.

Talukdar, P.K., et al., 2018. Parametric analysis of model savonius hydrokinetic turbines through experimental and computational investigations. Energy Convers. Manage. 158, 36–49.

Tian, W., et al., 2015. Computational fluid dynamics prediction of a modified Savonius wind turbine with novel blade shapes. Energies 8 (8), 7915–7929.

Wenehenubun, F., Saputra, A., Sutanto, H., 2015. An experimental study on the performance of savonius wind turbines related with the number of blades. Energy Procedia 68, 297–304.

Yaakob, O., Ahmed, Y.M., Ismail, M.A., 2012. Validation study for savonius vertical axis marine current turbine using CFD simulation. In: The 6th Asia-Pacific Workshop on Marine Hydrodynamics-APHydro2012.

Zhou, T., Rempfer, D., 2013. Numerical study of detailed flow field and performance of savonius wind turbines. Renew. Energy 51, 373–381.